Low-frequency vibrational properties of nanocrystalline materials: Molecular dynamics simulations of two-dimensional systems

Catherine Hudon,[1,*] Ralf Meyer,[2,†] and Laurent J. Lewis[1,‡]
[1]*Département de Physique et Regroupement Québécois sur les Matériaux de Pointe (RQMP), Université de Montréal, C.P. 6128, Succursale Centre-Ville, Montréal, Québec, Canada H3C 3J7*
[2]*Theoretische Tieftemperaturphysik, Universität Duisburg-Essen, 47048 Duisburg, Germany*
(Received 21 February 2007; revised manuscript received 29 May 2007; published 12 July 2007)

The low-frequency vibrational density of states (VDOS) of two-dimensional nanocrystalline materials is studied within the framework of molecular-dynamics simulations. The partial VDOS for different categories of atoms (as determined from their local environments), as well as the local (on-site) VDOS, is calculated. It is shown that the low-frequency spectrum exhibits a sequence of three distinct regimes below a critical density ρ^*, a direct consequence of the length-scale separation in the material: a first regime, at the lowest frequencies, corresponding to the elastic limit; a second (intermediate) regime, associated with the weak connectivity of the material under ρ^* and which does not necessarily show a two-dimensional behavior; a third regime, associated with grain modes and characteristic of a usual Debye solid. The intermediate regime is found to disappear above ρ^*. It is further demonstrated that the excess vibrational modes in the upper low-frequency regime arise mainly from grain-boundary atoms, while the other two regimes are related to the presence of pores in the materials.

DOI: 10.1103/PhysRevB.76.045409 PACS number(s): 63.50.+x, 63.22.+m, 81.07.Bc, 71.15.Pd

I. INTRODUCTION

It is well known that nanostructured materials possess unique mechanical and structural properties. For example, the large proportion of grain boundaries in nanocrystalline (NC) materials—obtained by assembling a large number of nanometer-scale grains—influences thermal quantities such as heat capacity, vibrational entropy, and Debye temperature. Knowledge of the vibrational density of states (VDOS) is crucial to understanding these novel properties. It has been established experimentally[1–8] and numerically[9–14] that the VDOS of NC materials is enhanced both at high and at low frequencies compared to their bulk counterparts. The excess modes at high frequencies have been attributed to phonon lifetime broadening[2,3,5] and shown to originate from strongly localized vibrations at grain boundaries.[15] In contrast, the enhancement at low frequencies is not well understood; in particular, there is no agreement on the precise value of the exponent of the observed power-law behavior. These modes have been shown to originate from vibrations of atoms at surfaces[10,12] or at grain boundaries.[7,13,14] Also, it has been proposed that the low-frequency VDOS of the excess modes scales either linearly with frequency[4,10,12] or with an exponent between 1 and 2,[11,13] suggesting a reduced dimensionality effect. Other studies have, however, found the low-frequency VDOS to obey the "normal" Debye behavior $g(\omega) \sim \omega^{d-1}$, where d is the spatial dimension.[2,3,6,7]

In the present work we investigate the origin of the low-frequency excess modes in NC materials as well as the specifics of the power-law behavior in these systems. To this effect, we have performed molecular-dynamics (MD) simulations of several two-dimensional NC model configurations containing $\sim 1 \times 10^6$ atoms or more. Two-dimensional systems were chosen because they allow larger length scales to be investigated compared to three-dimensional models. This is necessary to reach the long-wavelength regime which is of interest here (and to recover the elastic limit); the corresponding study in three dimensions would require a 1000-fold larger system, making the problem practically untractable.

Our calculations reveal unexpected features. Anticipating our results, we find the low-frequency VDOS to exhibit a sequence of three distinct regimes. At very low frequencies ("lower low-frequency regime," hereafter referred to as "I"), the elastic limit, whereby the system can be regarded as a purely elastic, homogeneous medium, is recovered. In the "intermediate low-frequency regime" ("II"), inhomogeneous modes that are not Debye-like are found; the extent of this regime decreases with increasing density and its upper limit is directly related to the grain size. The "upper low-frequency regime" ("III") is associated with grain-boundary modes and scales as a normal two-dimensional system—viz., linearly. The existence of these regimes is a direct consequence of the length-scale separation in nanocrystalline materials. At sufficiently long wavelengths, the nanocrystalline system acts as a homogeneous medium with reduced sound velocity compared to the ideal crystal. As the wavelength approaches the size of the grains and for systems not too dense, the phonons are strongly affected by the porous structure of the material, giving rise to the intermediate regime. Modes with even smaller wavelength—less than the size of the grains—are unaffected by the grain structure since such modes "see" mainly the homogeneous crystalline structure inside the grains. The intermediate regime is found to vanish at a density at which the material is sufficiently connected. This implies that not only the grain size, but also the density influences the thermal properties of nanocrystalline materials.

TABLE I. Initial configurations for the aggregation of nanoparticles into nanocrystalline materials; r is the radius of the clusters, N_{cl} the number of clusters, and N_{at} the number of atoms in the clusters. On average, $\bar{r} \approx 8.4$ and $\bar{N}_{at} \approx 223$ for NC-A and $\bar{r} \approx 9.4$ and $\bar{N}_{at} \approx 278$ for NC-B.

NC-A: 1 413 988 atoms			NC-B: 999 720 atoms		
r	N_{cl}	N_{at}	r	N_{cl}	N_{at}
5	1270	73	6	720	105
8	3810	182	9	2160	236
12	952	414	13	540	490
16	318	735	17	180	832

II. COMPUTATIONAL DETAILS

A. Model

The VDOS are calculated as described in Sec. II B. To generate the trajectories (in time) required for this, we use MD simulations. As mentioned above, our NC models are two dimensional, thus allowing very large systems to be dealt with and, as a consequence, much better statistics to be obtained, which turns out to be crucial for the range of frequencies we are interested in. While such models are of course not truly representative of real materials, we expect the physics to be comparable to that of three-dimensional systems, duly taking into account the dimensionality. Our approach should thus be viewed as "generic," providing the essential physics underlying the problem, not the details for a particular material. In this same spirit, the atoms are chosen to interact via a Lennard-Jones potential adjusted so as to vanish at the cutoff distance r_c:

$$U_{LJ}(r) = \begin{cases} 4\epsilon\left[\left(\frac{\sigma}{r}\right)^{12} - \left(\frac{\sigma}{r}\right)^{6} - \left(\frac{\sigma}{r_c}\right)^{12} + \left(\frac{\sigma}{r_c}\right)^{6}\right] & \text{if } r < r_c, \\ 0 & \text{if } r \geqslant r_c, \end{cases} \tag{1}$$

where ϵ is the well depth and σ is the atomic diameter; here, we set $r_c = 2.5\sigma$. The latter value—which encompasses the first three neighbor shells on a triangular lattice—is often used in generic simulations because the potential and the associated force are close to zero at this point. Evidently, this allows a considerable reduction of the computational load, while affecting very little the physics of our problem since the low-frequency vibrations are dominantly determined by the elastic properties of the model, not by the exact form of the potential. In this work, all results are reported in reduced units—i.e., ϵ for energy and σ for length—so that temperature is expressed in units of ϵ/k_B, ϵ/σ^3 for pressure, and $(m\sigma^2/\epsilon)^{1/2}$ for time. For a typical metal, $\epsilon \sim 1$ eV and $\sigma \sim 2-3$ Å. All simulations were carried out with a time step of 0.01 (~ 2 fs) and at $T = 0.025$ (~ 300 K). The Parrinello-Rahman[16] and Nosé-Hoover[17] algorithms were used to simulate constant-pressure and constant-temperature conditions.

The numerical approach used to construct the nanocrystalline models, akin to pressure-assisted nanoparticle sintering, is described in Ref. 14. This method allows systems with varying degree of densification to be generated; in comparison, an approach based on the Voronoi construction (used, e.g., in Refs. 9 and 15) only yields very dense model structures. Both methods are, however, found to provide very similar VDOS for compact models.[13] To initiate the construction of the NC models, we generate a number of isolated circular nanoparticles with diameters in the range 2.5–9 nm, the atoms initially lying on a perfect triangular lattice. These are first equilibrated over 75 000 simulation steps at $T = 0.025$, after which copies are distributed at random (and with random orientations) in a square box having twice the area of the corresponding crystalline lattice. The size distribution of the nanoparticles was chosen to resemble the corresponding experimental distribution. Once assembled, the nanoparticles quickly aggregate (over about 50 000 simulation steps) and form a loose powder. A series of configurations with higher densities can then be obtained by running at increasingly higher pressures (see below). For the purpose of the present study, two different series of samples ("NC-A" and "NC-B") were constructed, as summarized in Table I; these contain 1 413 988 and 999 720 atoms, respectively. We note that, on average, the grain size in sample NC-A is smaller than in NC-B; the difference will be used to characterize the various frequency regimes.

The densification cycle proceeded as follows. First, in both cases (NC-A and NC-B), the initial aggregation stage mentioned above was followed by a "predensification" run at pressure $P = 0.07$ (~ 70 MPa) for a further 50 000 steps. The pressure P_{max} was then increased gradually (cf. Table II); for each pressure, the systems were run over 100 000 simulation steps, in each case restarting from the previous configuration. Next, for each intermediate configuration (i.e., each value of P_{max}), the pressure was gradually reduced to zero in steps of 0.05, running over 2500 time steps in each case. Finally, the models were relaxed at zero pressure during another 100 000 simulation steps. The configurations so obtained are listed in Table II where we also give the relative density ρ—that is, the actual density of the system divided by the density of the corresponding crystalline material. The resulting nanocrystalline systems are "realistic" in the sense that they exhibit a porous structure quite similar to that observed experimentally; in particular, the porosity is found in real samples (consolidated from clusters at room temperature) to vary from less than 5% to about 25%.[18]

B. Calculation of the VDOS

The VDOS were calculated in two different ways. First, we used the Fourier transform of the velocity autocorrelation function[19] (VACF):

TABLE II. Maximum applied pressure P_{max} and relative density ρ of the samples considered in the present study.

NC A			NC B		
Sample	P_{max}	ρ	Sample	P_{max}	ρ
A1	0.2	0.74	B1	0.2	0.74
A1.1	0.33	0.77	B2	0.4	0.80
A2	0.4	0.80	B3	0.6	0.86
A2.1	0.5	0.82	B4	0.9	0.89
A3	0.6	0.84	B5	1.2	0.92
A4	0.8	0.87	B6	1.5	0.94
A5	1.0	0.89	B7	1.8	0.96
A6	1.2	0.91	B8	2.2	0.97
A7	1.4	0.93			
A8	1.6	0.94			
A9	1.8	0.95			
A10	2.0	0.96			
A13	2.5	0.97			

$$C_{vv}(t) = \langle \vec{v}(0) \cdot \vec{v}(t) \rangle. \tag{2}$$

The VACF was extracted directly from the MD simulation; in practice, we averaged over 2048 configurations (NC-A) or 4096 configurations (NC-B) and over 15 different runs (consecutive MD simulations) in order to obtain reliable statistics. The contributions to the VDOS may be sorted according to the local environments of the atoms. Here, each atom was given an "environment label" determined using the common neighbor analysis (CNA) method:[20] "perfect" for atoms with a perfect triangular environment at least up to second nearest neighbors, "good" for atoms which are perfect up to first nearest neighbors only, and "surface" for atoms with a coordination number $Z<5$; atoms that do not fit in any of these categories are labeled "GB" (grain boundary). Figure 1 shows the results of these assignments for a typical configuration (part of the NC-B4 sample).

The VACF method, however, does not easily allow investigating the local (on-site) VDOS associated with particular atoms. In order to do this, we used the on-site Green's function method and a recursion technique, as was done previously for the high-frequency spectra of nanocrystalline materials.[15] We briefly recall the method[21] here. The Green's operator for frequency ω is given by

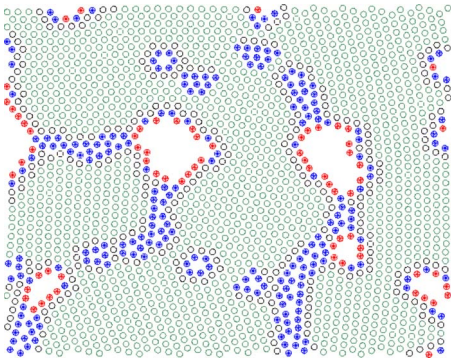

FIG. 1. (Color online) Part of the NC-B4 sample (relative density of 0.89) showing the different atom types: green=perfect, black=good, blue=GB, and red=surface.

$$[\hat{G}]_{ij}^{\mu\nu}(\omega) = [(\omega^2 \hat{I} - \hat{D})^{-1}]_{ij}^{\mu\nu}, \tag{3}$$

where $\hat{I}$ is the identity matrix and $\hat{D}$ the Hessian matrix of rank $2N$, N being the number of atoms in the system. The indices μ and ν represent the phonon polarization directions, and i and j vary from 1 to N. This operator is related to the local density of states $g_{i\mu}(\omega)$ as follows:

$$g_{i\mu}(\omega) = -\frac{\omega}{\pi} \lim_{\epsilon \to 0^+} \mathrm{Im}[G_{ii}^{\mu\mu}(\omega^2 + i\epsilon)]. \tag{4}$$

It can be shown that the on-site Green's function of a particular atom i, $G_{ii}^{\mu\mu}$, can be written approximately as an n-level continued fraction:

$$G_{ii}^{\mu\mu}(\omega) \cong \cfrac{1}{\omega^2 - a_0 - \cfrac{b_1^2}{\omega^2 - a_1 - \cfrac{b_2^2}{\ddots \cfrac{}{\omega^2 - a_{n-1} - b_n^2 t(\omega^2)}}}}, \tag{5}$$

where $t(\omega^2)$ is the square-root terminator[22] given by

$$t(\omega^2) = \frac{1}{b_\infty}\left[\left(\frac{\omega^2 - a_\infty}{2b_\infty}\right) - i\sqrt{1 - \left(\frac{\omega^2 - a_\infty}{2b_\infty}\right)^2}\right]. \tag{6}$$

The coefficients a_i and b_i are, respectively, the diagonal and off-diagonal elements of the tridiagonal symmetrical form of the Hessian matrix, obtained using the Lanczos algorithm,[23] while a_∞ and b_∞ are the values of a_i and b_i after n iterations, with $n \ll 2N$. The initial state (of norm unity) for starting the Lanczos's algorithm is set to

$$v_1 = (0, \ldots, 0, 1, 0, \ldots, 0)^T, \tag{7}$$

where the (unique) nonzero entry corresponds to the atom and polarisation for which the on-site VDOS is sought. The use of the square-root terminator is motivated by the convergence (in less than n iterations) to finite values of the a_i and b_i, so that the coefficients a_p and b_p for $p \geqslant n$ can be replaced by a_∞ and b_∞. In practice, we set $n=5000$; such a high value is necessary to recover the low-frequency elastic limit accurately. The coefficients a_∞ and b_∞ are taken by averaging over the last 100 values. In order to eliminate as much as possible the "contamination" from finite-temperature contributions, the atomic positions are first relaxed to their local minima using molecular statics.

III. RESULTS

A. Low-frequency VDOS

1. General features

We discuss first the overall features of the VDOS obtained by the Fourier transform method. Figure 2 shows the total

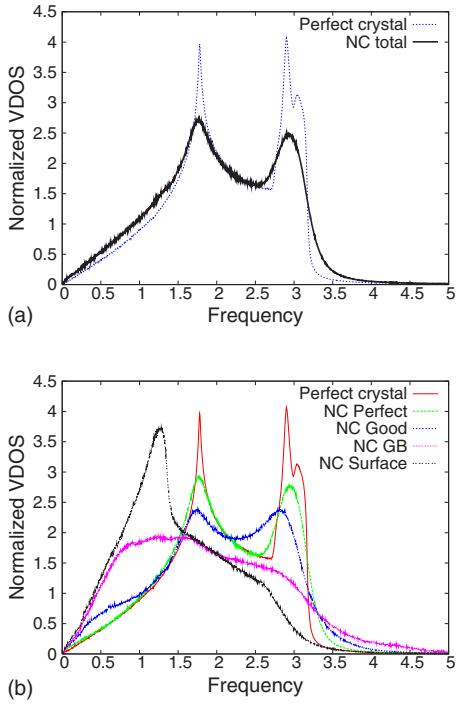

FIG. 2. (Color online) (a) Normalized VDOS for model NC-A5 and the corresponding perfect crystal and (b) contributions of the different types of atoms.

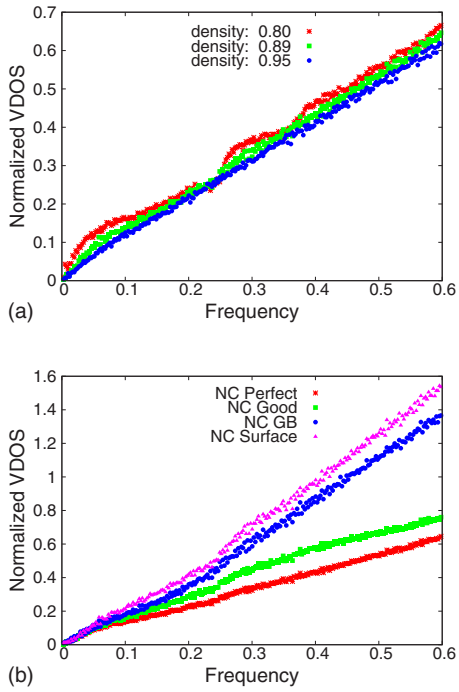

FIG. 3. (Color online) Low-frequency VDOS (a) for models NC-A2, NC-A5, and NC-A9, with densities ρ=0.80, 0.89, and 0.95, respectively, and (b) partial VDOS for the different categories of atoms in sample NC-A5.

VDOS as well as the contributions from the different types of atoms in model NC-A5, which is typical of our set of samples. For comparison, the VDOS of a perfect crystal (triangular lattice) containing approximately the same number of atoms is also shown. The results are consistent with other studies.[13] As expected, the partial VDOS for "good" atoms is intermediate between that for "perfect" and "GB" atoms; within the interior of the grains, the VDOS is similar to that for the bulk crystal. [In this and other figures, "frequency" is defined as $\omega/(2\pi)$.]

We focus now on the low-frequency part of the vibrational spectrum, displayed in Fig. 3(a) for three different samples (NC-A2, NC-A5, and NC-A9, with densities ρ =0.80, 0.89, and 0.95, respectively) and in Fig. 3(b) for sample NC-A5 for the different categories of atoms. We find that below some "critical" density ρ^*, the low-frequency VDOS exhibits three distinct regimes which we will refer to as "lower," "intermediate," and "upper" (or as "I," "II," and "III"), respectively; this is shown more clearly in Fig. 4 for sample NC-A5. For our two nanocrystalline models, we estimate that ρ^* is about 0.93. Above ρ^*, the intermediate regime vanishes. This behavior is observed for the total VDOS as well as for the different categories of atoms, as can be seen in Fig. 3(b). The VDOS in regimes I and III scales linearly with frequency for all NC models, as illustrated in Fig. 4; the behavior of the intermediate regime will be discussed in the next section. For regime I, the linear dependence is related to the fact that, at low frequency, vibrations are expected to be long-wavelength, acoustic waves and thus to scale as ω^{d-1}, d being the spatial dimension of the system. As for regime III, it will be shown below that the low-frequency bound (ω_{c2}) is determined by a characteristic length of the size of the grains. We thus expect the system to behave like a continuous elastic body below this length scale and the VDOS in regime III to exhibit a Debye behavior, as we indeed observe. In the presence of structural disorder, this description in terms of continuum elasticity must break down at some scale associated with the characteristic length below which there are inhomogeneities in the displacement field.[24,25] Actually, the translational invariance necessary for continuum theory to apply is lost due to the strong anisotropy of the system at some length scale, which gives rise to the intermediate regime II; there is consequently no reason to believe that the observed intermediate regime in the VDOS of our nanocrystalline models should also scale linearly.

This pattern—the scale separation in the low-frequency VDOS—shows similarities with the dynamics of some dis-

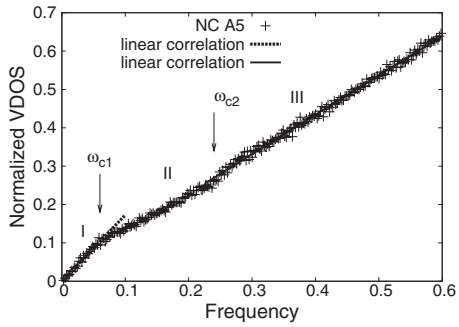

FIG. 4. Low-frequency VDOS for model NC-A5 (ρ=0.89); ω_{c1} and ω_{c2} are the crossover frequencies between regimes I, II and II, III, respectively. The lines are linear fits to the VDOS in regimes I and III.

ordered solids (e.g., aerogels,[26,27] powders,[28–30] jammed packings of particles,[31] fractal aggregates,[32] and amorphous materials[24,25]). In some of these cases,[26,27,30,32] the results are well accounted for by the fracton theory,[33] which shows that there is a crossover in the VDOS from propagating phonons to more localized modes called fractons. For powders, which possess unusual thermal properties at low temperature, Rutherford *et al.*[28] have proposed that the elastic regime exists only for characteristic lengths larger than $20D$, D being the diameter of the particles. These authors further assume that there exists inhomogeneous modes on the length scale of a few powder grains that have a constant VDOS, while for length scales smaller than D the modes are again Debye phonons (and the VDOS scales quadratically with frequency); the nature of the inhomogeneous modes, however, remains unclear. In contrast, Maliepaard *et al.*[29] proposed that sintered metal powders could be described as percolating systems, thus establishing an analogy between the transition from the elastic regime to the inhomogeneous modes and the fracton edge.

For jammed packing of particles approaching the unjamming transition,[31,34–36] it has been shown that there exists a correlation length ξ separating two regimes in the low-frequency VDOS; ξ is found to decrease with density and to diverge at some value ρ_c below which the system loses its mechanical stability (jamming-unjamming transition). At ρ_c, the low-frequency VDOS is a nonzero constant ("plateau") for all frequencies down to zero. For $\rho > \rho_c$, the system behaves as a Debye solid at lower frequencies, crossing over to a ρ_c-like solid at the frequency associated with ξ. No evidence for a fractal behavior was found. The plateau of excess low-frequency modes in the VDOS above ρ_c has been related to a particular set of soft modes; it has been demonstrated that these are a necessary consequence of the weak connectivity[35,36] (related to the number of contacts) of the system. The similarity of these results with the pattern observed in our systems suggests that nanocrystalline materials could perhaps be regarded as weakly connected mechanical systems, at some length scale greater than the grain size and at sufficiently low density. We expand on this idea in the next section and demonstrate that this is indeed the case.

2. Quantitative analysis

Following the above discussion, we write the low-frequency VDOS as

$$g_{LF}(\omega) = \begin{cases} k_1 \omega^{d-1}, & 0 < \omega < \omega_{c1}, \\ k_2(\omega - \omega_{c1})^{\tilde{d}-1} + \sigma_1, & \omega_{c1} < \omega < \omega_{c2}, \\ k_3(\omega - \omega_{c2})^{d-1} + \sigma_2, & \omega_{c2} < \omega < \omega_{max}, \end{cases} \quad (8)$$

where the constants σ_1 and σ_2 are given by

$$\sigma_1 = k_1 \omega_{c1}^{d-1}, \quad (9)$$

$$\sigma_2 = \sigma_1 + k_2(\omega_{c2} - \omega_{c1})^{\tilde{d}-1}, \quad (10)$$

and ω_{c1} and ω_{c2} are the crossover frequencies defined in Fig. 4; ω_{max} is the maximum frequency for the low-frequency regime, which we set to 0.6. We denote by $\tilde{d}$ the exponent

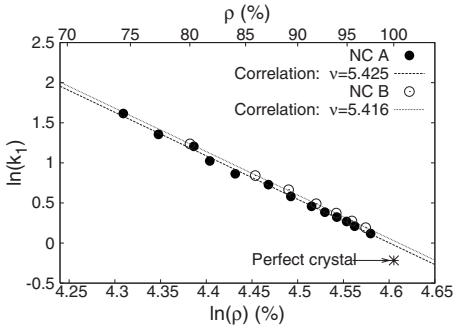

FIG. 5. The coefficient k_1 as a function of density for the total VDOS of the two NC models.

that describes the power-law behavior in regime II, which need not be equal to d. Since regime II vanishes for systems with densities above ρ^*, $\tilde{d}=d$ and $k_2=k_3$ in this case. As will be discussed below, the vibrational regimes are associated with different length scales l as follows. For $l > \xi$, with ξ a characteristic (or correlation) length of the order of the size of a few grains (a is the size of a single grain), the system behaves as an elastic continuum; this is regime I. For $l < a$, the vibrational properties are dominated by single grains; regime III is a "grain-mode" regime. Regime II corresponds to $\xi > l > a$ and is thus "intermediate." Of course, the crossovers between the various regimes are not abrupt because the grains are distributed in size.

As explained above, regime I is associated with the continuum limit. For a two-dimensional Debye solid we have, for $g(\omega)$ normalized,[37]

$$k_1 \sim \frac{A_0}{v_s^2}, \quad (11)$$

where A_0 and v_s are the area per atom and the sound velocity, respectively. The dependence of k_1 on density, $k_1 \sim \rho^{-\nu}$ (which defines the exponent ν), is shown in Fig. 5. The decrease of k_1 with density is well accounted for by the concomitant increase of the sound velocity, $v_s \sim \rho^{(\nu-1)/2}$, and the decrease of the area, $A_0 \sim \rho^{-1}$. The same scaling exponent is obtained for our two models—viz., $\nu \sim 5.4$. This is within the range of values for metallic powders (Ref. 29) ($\nu \sim 3$) or liquid argon in the metallic phase ($\nu \sim 7$) (see Ref. 38 and references therein). We note that k_1 is the same for the partial (atom-type) VDOS except for a small difference arising from the parameter A_0 for undercoordinated atoms (data not shown): k_1 for GB and surface atoms is slightly larger than for perfect and good atoms. We note also that the value of k_1 does not approach that for the perfect crystal in the limit $\rho \to 1$; this is due to the fact that it is very difficult to reach the perfectly ordered state by compaction.

We now turn to the upper low-frequency regime III which spans the largest frequency window. We have seen above that the VDOS scales linearly with ω (for $d=2$) in this regime. Figure 6 presents the variation of k_3 with density. This parameter is essentially the same for the two models—i.e., is not affected significantly by the size of the grains, except in the case of surface atoms, which is likely related to the fact

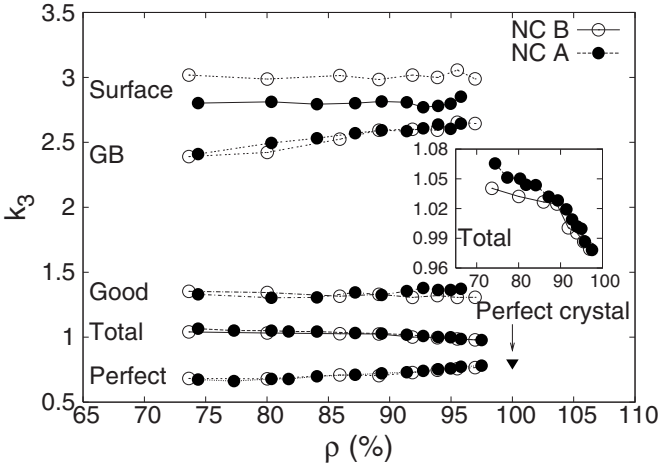

FIG. 6. The coefficient k_3 as a function of density for the total and the partial VDOS of the two NC models. Inset: k_3 vs density for the total VDOS.

that the curvature of the grains for model NC-A is on average larger than that in NC-B: it is indeed well known that the morphology of nanoparticles have an effect on their VDOS.[39] Also, a small enhancement of the modes for the total VDOS in this regime with decreasing grain size is evident from the inset in Fig. 6; this is directly related to the increased presence of grain boundary atoms in the model with smaller grains (NC-A), as we discuss below.

The overall value of k_3 depends only weakly on density, decreasing slightly; our calculations show that this results from the small decrease of the number of GB atoms with compaction, not of the larger variation of the number of surface atoms. For "perfect" atoms, we observe a weak increase, k_3 approaching the value for the perfect crystal. By analogy with the Debye theory [cf. Eq. (11)], this could indicate that the interatomic distances for perfect atoms increases with compaction, suggesting a reduced stress inside the grains due to the increase of the grain size and the transformation of free surfaces into grain boundaries at higher densities. The value of k_3 for GB atoms exhibits a larger variation with ρ. As we will see in Sec. III B, the low-frequency VDOS for properly coordinated GB atoms ($Z=6$) is substantially larger than that for undercoordinated GB atoms. The number of these respectively increase and decrease with density, thus accounting for the observed variation of k_3. This is consistent with the observation that the thermal properties of NC materials not only depend on the grain size, but also on the microstructure (or the density) of the grain boundaries.[40]

The lower-frequency limit of regime II, ω_{c1}, corresponds to a correlation length ξ of the order of the size of a few grains, as can be deduced from the value of the sound velocity in regime I. (In contrast, as we will see below, ω_{c2} corresponds to a correlation length $\sim$ the size of a single grain.) The system is quite inhomogeneous on this scale and there is consequently no reason to believe that regime II may be described by a linear power-law scaling as is the case of regime I. The frequency ω_{c1} is thus associated to the length scale at which continuum theory ceases to apply; as in the case of jammed packings of particles,[31,35] it should therefore

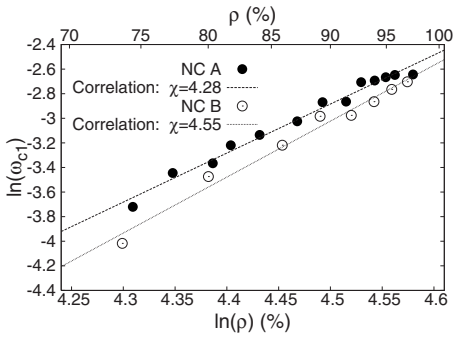

FIG. 7. The frequency ω_{c1} as a function of density for the total VDOS of the two NC models.

scale with ρ. This is verified in Fig. 7 where ω_{c1} is shown to be well described by a power-law dependence on ρ, $\omega_{c1} \sim \rho^{\chi}$, with χ depending only slightly on grain size ($\chi_{\text{NC-A}}=4.28$ and $\chi_{\text{NC-B}}=4.55$). From the dispersion relation for phonons[41] we can write $\omega_{c1} \approx \frac{v_s}{\xi}$, with v_s the sound velocity. ω_{c1} should therefore be a little smaller for NC-B than for NC-A since the latter has smaller grains and $\xi\sim$ a few grains; this is indeed what we find. From the above relations we have

$$\xi \sim \rho^{-[(2\chi-\nu+1)/2]}. \tag{12}$$

For our two NC models, we obtain $\xi \sim \rho^{-\tau}$, with $\tau \approx 2.2$, consistent with the fact that the correlation length decreases with density.[25] As a consequence, we would expect ξ to diverge as density is lowered, as also suggested for jammed packings of particles.[31] In practice, we do not have a density at which ξ diverges [i.e., for which $g(\omega) \neq 0$ at $\omega=0$] (Ref. 36) because the density of our systems is still well above the value for mechanical stability to break down. One may conjecture that ω_{c1} could possibly be associated with the theoretically predicted[33] "transition" from phonons to fractons; we will see below that this is not the case here.

We now turn to the crossover from regime II to regime III. ω_{c2} corresponds to a characteristic length typical of the size of the grains, and thus regime III is associated with grain modes. The dependence of ω_{c2} on density for our two families of samples is displayed in Fig. 8. We find, indeed, that ω_{c2} is smaller for the sample with larger grains (NC-B). We observe, further, that ω_{c2} is essentially constant with density,

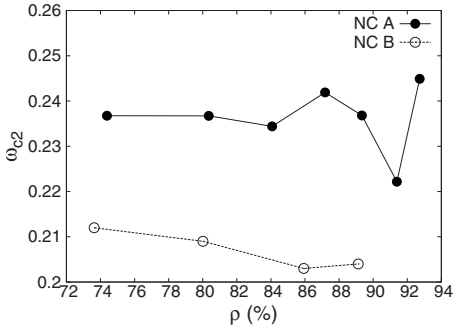

FIG. 8. The frequency ω_{c2} as a function of density for the total VDOS of the two NC models.

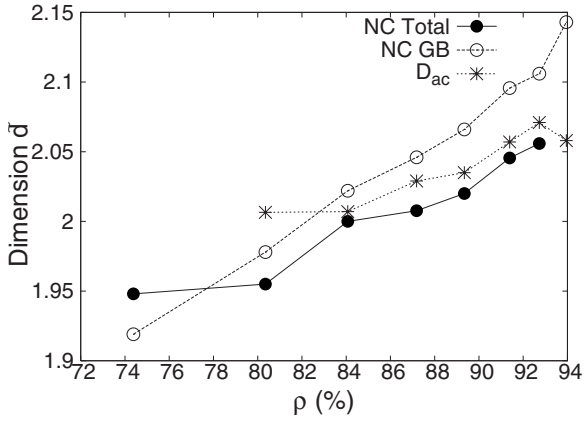

FIG. 9. $\tilde{d}$ as a function of density for the total and the GB VDOS of model NC A compared with the acoustic fractal dimension D_{ac} (see text for details).

except perhaps for a small drop at larger values of ρ which likely results from the coalescence of grains upon compaction.

As a final point concerning the ω_c's, we note in Fig. 3 the presence of "humps" upon going from one regime to another; these are related to the coexistence of two regimes about the crossover frequencies. In particular, the hump at ω_{c2} is due to the fact that the distribution of grain sizes has a finite width. These humps become less important with increasing density because the intermediate regime becomes less important. We define ω_e as the frequency at which the coexistence ceases for the crossover between regimes II and III; at sufficiently high density, $\omega_e = \omega_{c2}$.

We consider now the variation of $\tilde{d}$, with density; this is shown in Fig. 9 for model NC-A (for which statistics are better) for both the total VDOS and the GB VDOS. $\tilde{d}$ does not differ appreciably from d (=2), but there is nevertheless a nontrivial increase with density, indicating a small dependence on the microstructure. We can relate $\tilde{d}$ to the spectral dimension $\bar{d}$—that is, the generalization of d (Euclidean dimension, here 2) to noncrystalline structures; this is equivalent to the fracton dimension for fractal systems.[33] The fracton theory provides $\bar{d} = \frac{D_f}{\alpha}$ (with $\bar{d} < d$), where D_f is the fractal dimension and α is a constant related to the nature of the fractal, or more precisely to the scaling exponent for diffusion. Chadwick[42] proposed that the VDOS of nanocrystalline iron could be described in terms of fractons, implying of course that the atomic structure is itself fractal. Our results for $\tilde{d}$ are no evidence for a fractal structure. However, as far as vibrational properties are concerned, the relevant length is the acoustic correlation length and the relevant fractal dimension is the acoustic fractal dimension, which is associated with the connectivity of the structure rather than the mass distribution.[27] It is thus reasonable to relate the connectivity to the porous structure of our NC materials. We therefore calculated this quantity in order to obtain the acoustic fractal dimension D_{ac} (see the Appendix for details). From Fig. 9 it appears that D_{ac} scales the same way as $\tilde{d}$ with ρ—i.e., $\tilde{d} = \frac{D_{\mathrm{ac}}}{\tilde{\alpha}}$, with $\tilde{\alpha}$ approximately the same for all densities as in Ref. 26. However, the variations in $\tilde{d}$ are too small to conclude unambiguously that this relation is valid—i.e., that fracton theory applies in the present case.

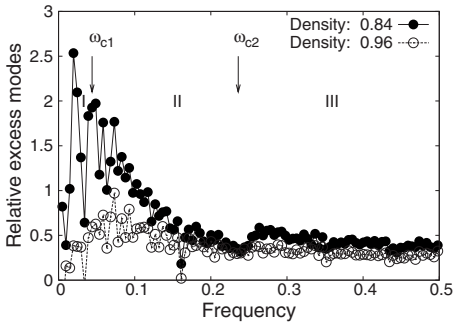

FIG. 10. Relative number of excess modes compared to the perfect crystal for two NC models with different densities 0.84 (NC-A3) and 0.96 (NC-A10). The value of ω_{c1} is for model NC-A3.

As for the coefficient k_2, we limit our discussion to the qualitative observation that it clearly increases with density (cf. Fig. 3). In short, the intermediate regime is "abnormal" and related to inhomogeneities in the structure. It is difficult to assess how it changes exactly with density and what happens when regime II vanishes because there are many parameters that change simultaneously with ρ [in particular ω_{c1}, $\bar{d}$, and the widths of the crossovers (or humps) between the three regimes].

To summarize this section, we have shown that regimes I and II depend strongly on density, while regime III does not. This can also be seen in Fig. 10 where we plot the relative number of excess modes (compared to the crystal) for two NC-A samples. This figure also clearly demonstrates that the number of excess modes is larger for lighter materials in regimes I and II, while the differences are very small in regime III (and have been attributed above to the small decrease in the number of grain boundary atoms upon compaction). We see, further, that $g(\omega_{c2})$ is the same for both densities [see also Fig. 3(a)]. The variation of $g(\omega)$ with density in regime I is well explained by the increase of the sound velocity with increasing density. In regime III, the number of excess modes does not depend strongly on density, in agreement with earlier results[7,14] that show that the enhancement of low-frequency modes in nanocrystalline materials is due to the larger proportion of grain boundaries in comparison with polycrystalline materials—the nature of the grain boundaries in nanocrystalline materials is not fundamentally different in terms of the degree of disorder from that of polycrystals[43]—and not to some surface effects. However, we have demonstrated that, at very low frequencies, such surface effects do exist (if only because of variations in the velocity of sound). Actually, the weak connectivity of nanocrystalline materials (proportional to the degree of compaction) under ρ^*, on the scale of a few grains, strongly influences the behavior and the number of excess modes in the intermediate regime II, as demonstrated by Wyart *et al.*[35] for jammed packing of particles (or amorphous solids). Thus, we may speculate that regime II vanishes at the density at which the nanocrystalline material is sufficiently connected (i.e.,

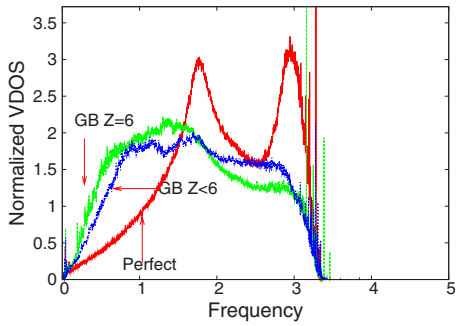

FIG. 11. (Color online) Normalized VDOS of sample NC-B3 obtained by the Green's function method. The partial VDOS for GB atoms is separated into fully coordinated ($Z=6$) and undercoordinated ($Z<6$) atoms.

the porous structure becomes negligibly small) that it behaves as a two-dimensional solid.

B. Local (on-site) VDOS

From the above discussion, we are led to conclude that the vibrational modes in the intermediate regime are strongly influenced by the porosity of the material. In order to assess this, we computed the local (on-site) VDOS, which provide a detailed, atomic-level picture of the distribution of excess modes. Figure 11 shows the VDOS obtained using the Green's function method for different types of atoms (averaged in each case over 1000 atoms chosen at random). The results are nearly identical to those obtained using the VACF method (cf. Fig. 2), except for the high-frequency tail which results from anharmonic terms in the finite-temperature MD calculations as noted earlier. We also note that the low-frequency VDOS for the GB atoms with perfect coordination ($Z=6$) is larger than that for undercoordinated atoms.

We present in Fig. 12 the on-site VDOS for a selected part of the NC-B3 model and for phonon energies in regime II (top) and far in regime III (bottom). The atoms are colored according to the logarithm of the value of the VDOS (see caption). These plots provide a summary of our earlier qualitative observations. In the intermediate regime II, the modes tend to be more intense near the surface of the pores; in the upper regime III, while still intense at the surface, they are also strongly present in grain boundaries not associated with the pores (i.e., free area). Thus, the intensity of the modes near the pores in regime III decreases with increasing frequency.

In order to quantify these observations we may calculate the relative contribution of selected atoms to the VDOS for fixed ω; for this purpose, we introduce the "contribution ratio," which we define as

$$\eta = \frac{\sum_{k} g_k(\omega)}{\sum_{j=1}^{N} g_j(\omega)}, \tag{13}$$

where $g_i(\omega)$ is the on-site VDOS at site i for frequency ω, N is the total number of atoms, and k represents the atoms for

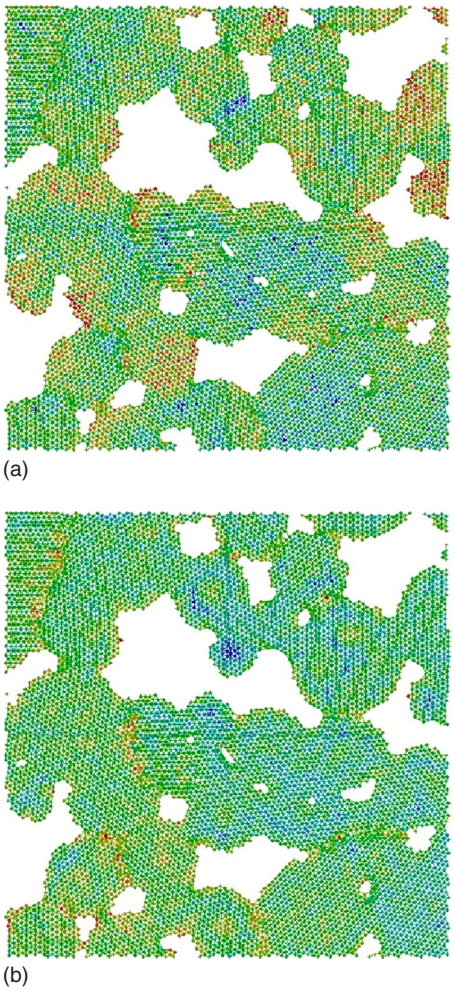

FIG. 12. (Color online) On-site VDOS for a selected part of sample NC-B3 in regime II (top, $\omega=0.15$) and regime III (bottom, $\omega=0.55$). The atoms are shaded according to the value (on a logarithmic scale) of the local VDOS. The scale goes from blue (low on-site VDOS) to red (high on-site VDOS).

which the relative contribution to the total VDOS is sought. The results are presented in Fig. 13 for two NC-B models, below and above the critical density. The upper two curves give the relative contribution of the atoms located at, or near (first and second neighbors), the surface of pores, while the bottom two curves are for atoms at grain boundaries which are not associated with free area. The calculations were done for exactly the same region of the two samples; the results are robust with respect to the definition of near-surface atoms (i.e., whether we include first, second, or third neighbors from the surface) and are reproducible for other (randomly selected) regions of the models. It is clear from this figure that the contribution ratio of the modes at grain boundaries which are *not* associated with free area increases with frequency. In contrast, the intensity of the modes near pores begins to decrease at some frequency close to the onset of regime III, after reaching a maximum value near the end of the intermediate regime, ω_{c2} or ω_e, the latter being defined as the frequency at which the crossover ("hump") ends; ω_e is lower for the denser sample (NC-B6) because the VDOS

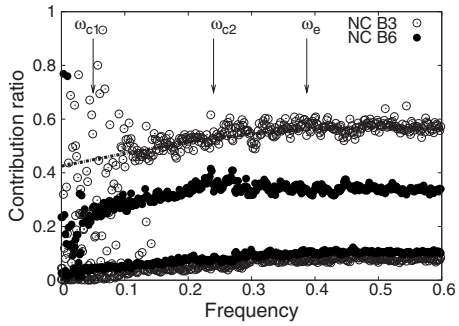

FIG. 13. Contribution ratio for a randomly selected region of models NC-B3 and NC-B6 as a function of frequency. ω_e is defined as in Sec. III A 2 for model NC-B6. The upper two curves are for atoms located at, or near, the surface of pores, while the bottom two curves are for atoms at grain boundaries which are not associated with free area. The line is a guide for the eye.

does not exhibit the hump resulting from the coexistence of regimes II and III.

In order to compare the relative contributions of atoms near a pore with those of atoms not associated with free area, we consider the normalized relative participation ratio—viz., η/N_η, with N_η defined as the number of atoms for which η is computed; the results are presented in Fig. 14 for model NC-B3. It is quite interesting that the two curves cross at ω_{c2}. This means again that, in the intermediate regime II, those atoms (or regions) that have the largest influence on the VDOS are those lying near a pore; in contrast, in regime III, the dominant modes are more localized in the grains and in grain boundaries not associated with free area. The fact that the number of such atoms remains essentially constant upon increasing the density demonstrates again why k_3 does not vary much with density. Actually, there is a slight increase with density which is compensated by a more important decrease of the number of atoms neighboring pores. Since the number of atoms located near pores decreases with density, it then becomes clear why the weight of excess modes in the intermediate regime also decreases. Summing up, the porous structure evidently influences the behavior of the low-frequency modes; its impact on the intermediate regime is clearly of great importance.

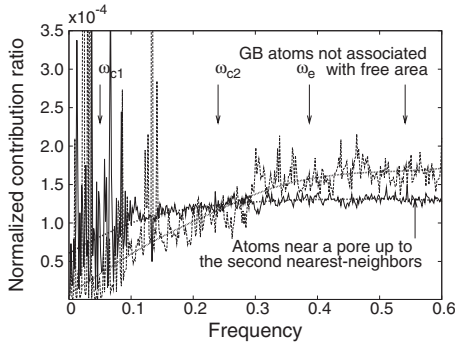

FIG. 14. Normalized contribution ratio for part of model NC-B3 as a function of the frequency. The lines are natural spline approximations to the data.

IV. SUMMARY

We have studied the low-frequency vibrational properties of model nanocrystalline materials within the framework of molecular-dynamics simulations. We have found the low-frequency spectrum of these materials to exhibit a sequence of two or three different regimes, depending on density: there exists a critical density ρ^*, depending only slightly on the average grain size, above which the intermediate regime vanishes. This regime, below ρ^*, crosses over from the usual elastic solid (regime I) at the frequency at which continuum theory ceases to apply; we have shown that it is intimately related to the weak connectivity of the material on the length scale of a few grains and that it does not show the normal two-dimensional behavior. The third regime is associated with grain modes and corresponds to the usual Debye solid. We have also shown that the excess modes in the last regime are due to the high number of grain-boundary atoms; in contrast, the excess modes in the first two regimes are related to the significant presence of free area (pores).

ACKNOWLEDGMENTS

This work has been supported by grants from the Natural Sciences and Engineering Research Council of Canada (NSERC) and the "Fonds Québécois de la Recherche sur la Nature et les Technologies" (FQRNT). R.M. thanks the "Deutsche Forschungsgemeinschaft" for support through SFB 445. We are indebted to the "Réseau Québécois de Calcul de Haute Performance" (RQCHP) for generous allocations of computer resources.

APPENDIX: CONNECTIVITY

We describe here how the connectivity of the NC models is computed. From algebraic topology, it is known that, in two dimensions, the connectivity number (or Euler characteristic) ζ of a given structure is given by:[44]

$$\zeta = n_c - n_h, \tag{A1}$$

where n_c and n_h are the number of connected components and the number of holes (i.e., pores), respectively. If the structure is regarded as a compact object with holes in it and assuming it is continuous on the atomic scale, then $\zeta = 1 - n_h$. The acoustic fractal dimension $D_{\rm ac}$ is obtained from the relation $\zeta \sim R^{D_{\rm ac}}$. In order to calculate n_h (which depends on R), we need to determine the positions of the pores. To do this, we first subdivide the system into small cells (of length 0.28); to each we associate the atom which is closest. These are then used to identify surface atoms and free area. An atom is defined to be at the surface (of a pore) if there exists at least one cell associated to it at a distance larger than $r_p = 1.075$. A subcell is listed as free area if there are no atom closer than r_p. Once surfaces atoms have been identified, the pores are delimited using the Hoshen-Kopelman algorithm.[45] In order to locate the positions of the pores we identify, for each, that atom that is closest to the center O of the system. The radial distribution $n_h(R)$ can then be calculated by counting the number of pores that lie within a circle of radius R from O.

*catherine.hudon@UMontreal.CA
†Ralf.Meyer@uni-due.de
‡laurent.lewis@UMontreal.CA

[1] J. Trampenau, K. Bauszus, W. Petry, and U. Herr, Nanostruct. Mater. **6**, 551 (1995).
[2] B. Fultz, C. C. Ahn, E. E. Alp, W. Sturhahn, and T. S. Toellner, Phys. Rev. Lett. **79**, 937 (1997).
[3] H. Frase, B. Fultz, and J. L. Robertson, Phys. Rev. B **57**, 898 (1998).
[4] U. Stuhr, H. Wipf, K. H. Andersen, and H. Hahn, Phys. Rev. Lett. **81**, 1449 (1998).
[5] E. Bonetti, L. Pasquini, E. Sampaolesi, A. Deriu, and G. Cicognani, J. Appl. Phys. **88**, 4571 (2000).
[6] L. Pasquini, A. Barla, A. I. Chumakov, O. Leupold, R. Rüffer, A. Deriu, and E. Bonetti, Phys. Rev. B **66**, 073410 (2002).
[7] A. B. Papandrew, A. F. Yue, B. Fultz, I. Halevy, W. Sturhahn, T. S. Toellner, E. E. Alp, and H. Mao, Phys. Rev. B **69**, 144301 (2004).
[8] A. F. Yue, A. B. Papandrew, O. Delaire, B. Fultz, Z. Chowdhuri, R. M. Dimeo, and D. A. Neumann, Phys. Rev. Lett. **93**, 205501 (2004).
[9] D. Wolf, J. Wang, S. R. Phillpot, and H. Gleiter, Phys. Rev. Lett. **74**, 4686 (1995).
[10] A. Kara and T. S. Rahman, Phys. Rev. Lett. **81**, 1453 (1998).
[11] X. Hu, G. Wang, W. Wu, P. Jiang, and J. Zi, J. Phys.: Condens. Matter **13**, L835 (2001).
[12] D. Y. Sun, X. G. Gong, and X. Q. Wang, Phys. Rev. B **63**, 193412 (2001).
[13] P. M. Derlet, R. Meyer, L. J. Lewis, U. Stuhr, and H. Van Swygenhoven, Phys. Rev. Lett. **87**, 205501 (2001).
[14] R. Meyer, L. J. Lewis, S. Prakash, and P. Entel, Phys. Rev. B **68**, 104303 (2003).
[15] P. M. Derlet and H. Van Swygenhoven, Phys. Rev. Lett. **92**, 035505 (2004).
[16] M. Parrinello and A. Rahman, Phys. Rev. Lett. **45**, 1196 (1980).
[17] W. G. Hoover, Phys. Rev. A **31**, 1695 (1985).
[18] R. W. Siegel, *Nanomaterials: Synthesis, Properties and Applications* (Institute of Physics, Bristol, 1996), Chap. 9.
[19] M. P. Allen and D. J. Tildesley, *Computer Simulation of Liquids, Oxford Science Publications* (Oxford University Press, Oxford, 1987).
[20] J. D. Honeycutt and H. C. Andersen, J. Phys. Chem. **91**, 4950 (1987).
[21] M.-C. Desjonquères and D. Spanjaard, *Concepts in Surface Physics* (Springer, Berlin, 1996).
[22] R. Haydock, V. Heine, and M. J. Kelly, J. Phys. C **5**, 2845 (1972).
[23] C. Lanczos, J. Res. Natl. Bur. Stand. **45**, 255 (1950).
[24] F. Léonforte, A. Tanguy, J. P. Wittmer, and J.-L. Barrat, Phys. Rev. Lett. **97**, 055501 (2006).
[25] F. Léonforte, R. Boissière, A. Tanguy, J. P. Wittmer, and J.-L. Barrat, Phys. Rev. B **72**, 224206 (2005).
[26] J. Kieffer and C. A. Angell, J. Non-Cryst. Solids **106**, 336 (1988).
[27] E. Courtens and R. Vacher, Proc. R. Soc. London, Ser. A **423**, 55 (1989).
[28] A. R. Rutherford, J. P. Harrison, and M. J. Stott, J. Low Temp. Phys. **55**, 157 (1984).
[29] M.-C. Maliepaard, J. H. Page, J. P. Harrison, and R. J. Stubbs, Phys. Rev. B **32**, 6261 (1985).
[30] M. Hayashi, E. Gerkema, A. M. van der Kraan, and I. Tamura, Phys. Rev. B **42**, 9771 (1990).
[31] L. E. Silbert, A. J. Liu, and S. R. Nagel, Phys. Rev. Lett. **95**, 098301 (2005).
[32] T. Terao, A. Yamaya, and T. Nakayama, Phys. Rev. E **57**, 4426 (1998).
[33] S. Alexander and R. Orbach, J. Phys. (France) Lett. **43**, L625 (1982).
[34] C. S. O'Hern, L. E. Silbert, A. J. Liu, and S. R. Nagel, Phys. Rev. E **68**, 011306 (2003).
[35] M. Wyart, L. E. Silbert, S. R. Nagel, and T. A. Witten, Phys. Rev. E **72**, 051306 (2005).
[36] M. Wyart, S. R. Nagel, and T. A. Witten, Europhys. Lett. **72**, 486 (2005).
[37] N. W. Ashcroft and N. D. Mermin, *Solid State Physics* (Brooks-Cole, Belmont, MA, 1976).
[38] S. Munejiri, F. Shimojo, and K. Hoshino, J. Phys.: Condens. Matter **10**, 4963 (1998).
[39] G. A. Narvaez, J. Kim, and J. W. Wilkins, Phys. Rev. B **72**, 155411 (2005).
[40] L. H. Qian, S. C. Wang, Y. H. Zhao, and K. Lu, Acta Mater. **50**, 3425 (2002).
[41] T. Nakayama and K. Yakubo, *Fractal Concepts in Condensed Matter Physics* (Springer, Berlin, 2003).
[42] J. Chadwick, J. Phys. A **32**, 4087 (1999).
[43] P. M. Derlet and H. Van Swygenhoven, Phys. Rev. B **67**, 014202 (2003).
[44] M. S. Barbosa, L. da Fountoura Costa, and E. de Sousa Bernardes, Phys. Rev. E **67**, 061910 (2003).
[45] J. Hoshen and R. Kopelman, Phys. Rev. B **14**, 3438 (1976).